



Midlatitude atmospheric transient eddy feedbacks influenced ENSO-associated wintertime Pacific teleconnection patterns in two PDO phases

Cuijiao Chu¹ · Haibo Hu^{1,3} · Xiu-Qun Yang¹ · Dejian Yang²

Received: 3 June 2019 / Accepted: 13 January 2020 / Published online: 29 January 2020
© The Author(s) 2020

Abstract

The El Niño-Southern Oscillation (ENSO)-associated wintertime atmospheric teleconnection patterns in two Pacific decadal oscillation (PDO) phases are investigated using ERA-20C reanalysis data for 1950–2010. A strengthened ENSO-associated Pacific-North American (PNA) teleconnection pattern presents in PDO positive phase, while a West Pacific (WP) pattern over Northwestern Pacific and a squeezed PNA pattern coexist when ENSO occurs in PDO negative phase. The dynamical role of atmospheric transient eddy feedbacks to the teleconnection patterns are highlighted in the present study. When ENSO occurs in PDO positive phase, the uniform strengthened westerly jet anomalies downstream of the climatological main body of jet accompany with energetic transient eddy anomalies over Northeastern Pacific. The transient eddy feedbacks largely enhance and favor the strengthened PNA pattern. When ENSO occurs in PDO negative phase, the strengthened westerly jet anomalies appear to separate into two parts, one locating north of the climatological main body of jet and the other at the downstream. The accompanied transient eddy anomalies also split into two parts. Under such conditions, the transient eddy feedbacks are limited over Northeastern Pacific and favor a weak PNA pattern. However, the transient eddy anomalies over Northwestern Pacific strengthen, and the feedbacks also strengthen and largely contribute to the WP pattern. Moreover, the transient eddy anomalies over Northwestern Pacific seem to be anchored along the anomalously poleward strengthened oceanic subarctic frontal zone (SAFZ) in PDO negative phase. The enhanced atmospheric baroclinicity anomalies, coupled with the strengthened SAFZ, energize atmospheric transient eddy anomalies, and work as the potential maintenance in shaping the WP pattern.

Keywords Atmospheric teleconnection patterns · ENSO · PDO · Transient eddy feedbacks · Subarctic oceanic frontal zones

1 Introduction

El Niño-Southern Oscillation (ENSO), as the dominant pattern of interannual climate variability, greatly influences the atmospheric circulation and triggers a cascade of atmospheric teleconnections around the globe (e.g., Bjerknes

1969; Wallace and Gutzler 1981, hereafter WG81; Hoskins and Karoly 1981; Deser and Wallace 1990; Wang 2000). Particular attention has been devoted to the linkages between the ENSO and Pacific-North American (PNA) teleconnection pattern (e.g., Horel and Wallace 1981; Lau and Nath 1994; Alexander et al. 2002). The PNA teleconnection has the same sign of geopotential anomaly in the midlatitude North Pacific and southeastern North America and the opposite geopotential anomaly sign in northwestern North America. Other studies have shown the linkage between ENSO and western Pacific (WP) teleconnection pattern (e.g., Horel and Wallace 1981; Koide and Kodera 1999), which was confirmed as the third mode of singular value decomposition (SVD) between the geopotential height and sea surface temperature anomalies (SSTA) in boreal winter (The positive phase of WP pattern is defined when the northern height

✉ Haibo Hu
huhaibo@nju.edu.cn

¹ CMA-NJU Joint Laboratory for Climate Prediction Studies, Jiangsu Collaborative Innovation Center of Climate Change, School of Atmospheric Science, Nanjing University, Nanjing, China

² College of Oceanography, Hohai University, Nanjing, China

³ KLME & CIC-FEMD, NUIST, Nanjing, China

anomaly is positive, following the definition of WG81). The WP pattern is a meridional dipole pattern of atmospheric circulation anomalies at the middle/high latitudes of the Northwestern Pacific, related to the meridional shift of the Aleutian Low (Liu and Alexander 2007; Di Lorenzo et al. 2015), well known as the major pattern that modulates the East Asian winter monsoon (Takaya and Nakamura 2013). They are usually interpretable as the result of midlatitude stationary wave anomalies associated with the tropical heating related to ENSO and the dynamical adjustment between zonal mean flow and transient eddies both from the theoretical and modeling perspective.

However, the ENSO teleconnections magnitude and stability are changeable, and may be influenced by interdecadal variation of Pacific Decadal Oscillation (PDO) (Gershunov and Barnett 1998; McCabe et al. 2004). With observations of a major climate regime shift around the end of the 1970s, the PDO has been more and more recognized (e.g., Trenberth and Hurrell 1994; Mantua et al. 1997; Zhu and Yang 2003; Chu et al. 2014). The PDO exerts a remarkable effect on ENSO-associated atmospheric circulations. When ENSO and PDO are in phase (El Niño and PDO positive phase, or La Niña and PDO negative phase), a similar teleconnection pattern with the same sign generated by ENSO-Only and PDO-Only is overlapped and enhanced. However, when ENSO and PDO are out of phase (El Niño and PDO negative phase, or La Niña and PDO positive phase), ENSO-only and PDO-only generate a similar teleconnection pattern with opposite sign, causing cancellation of the anomalous circulation (Hu and Huang 2009). The associated teleconnection patterns are interpreted from the viewpoint of stationary Rossby wave energy dispersion from changeable tropical heating related to tropical SSTA distribution. The magnitude and spatial shift in the tropical convection associated with the anomalous tropical Pacific SSTA distribution plays an important role in the sensitivity of remote atmospheric response (Chu et al. 2018). The tropical convection tends to be stronger and more stable associated with the same sign of tropical SSTA when ENSO and PDO are in phase. However, it tends to be weaker associated with the opposite sign of tropical SSTA when ENSO and PDO are out of phase.

Less attention has been paid on the dynamical role of atmospheric synoptic-scale transient eddy feedbacks to the maintenance of PDO influenced ENSO-associated teleconnections. In midlatitude troposphere, the westerly jet and associated transient eddy activities are special features of atmospheric motions. The jet stream is considered large-scale circulation, while the transient eddy activities can be referred to as synoptic-scale eddies, also addressed as storm track activities. The relationship between mean flow and storm tracks appears to be “symbiotic” in nature (Cai and Mak 1990). Strong baroclinic conversion of the

available potential energy from the mean flow to the transient eddies coincides with the rapid growth in transient variance in the downstream (eastward) direction (Chang et al. 2002). In return, the midlatitude transient eddy feedbacks are recognized as an important role for understanding the generation and maintenance of the atmospheric circulation anomalies (e.g., Lau and Nath 1991; Ren et al. 2008). The synoptic-scale transient eddy activities influence the time-mean flow through the convergence of eddy heat and momentum fluxes. One objective of this study is to explore the midlatitude synoptic-scale transient eddy feedbacks in the ENSO-associated atmospheric teleconnection patterns in two PDO phases.

The associated atmospheric teleconnections may be a complex combination of different physical process including both internal eddy-mean flow interactions originated from remote tropical forcing and North Pacific local atmosphere–ocean interactions. While the ENSO emphasizes the influence associated with tropical Pacific SSTA, the PDO may stress on variation associated with extra-tropical Pacific SSTA. The basin-scale North Pacific SST variability is large near the strong SST gradients along the oceanic fronts, especially at decadal time scales (Nakamura and Kazmin 2003; Kwon et al. 2010). It is commonly considered that there are two major frontal zones: the subarctic frontal zone (SAFZ) near 42° N, and the subtropical front zones (STFZ) between 28° N and 32° N (Nakamura et al. 1997a, b). The SAFZ front with a strong SST gradient associated with western boundary currents and their extensions is usually much stronger than STFZ which is crossing almost the whole North Pacific basin (Nonaka et al. 2006). Observational evidence demonstrates that the oceanic front zones that mainly respond to the wind stress have an influence on the atmospheric circulation in North Pacific (two-way coupling, Qiu and Chen 2005; Xu et al. 2008, 2010; Frankignoul et al. 2011). The importance of SAFZ for tropospheric circulation in the free atmosphere has been recognized in recent decades (Nakamura et al. 2004, 2008; Yao et al. 2016). They argue that heat supply anchored by the subarctic frontal zone acts to maintain surface baroclinicity, and sustaining the atmospheric midlatitude storm. Major transient eddies are organized along or just at the downstream of the main oceanic frontal zones, and can be intensified as a response to enhanced SAFZ in sensitivity numerical experiments. In addition, observation and idealized numerical experiments indicate that enhanced STFZ strengthens meridional temperature gradient and thus atmospheric baroclinicity, inducing more active transient eddies with the acceleration of westerly jet (Zhang et al. 2017; Wang et al. 2018; Chen et al. 2019). With respect of the close relationship between oceanic frontal zones and variability of PDO, we extend the scope of the present study by investigating the possible connection of the

oceanic frontal zones and transient eddy activities in PDO influenced ENSO-associated teleconnections.

The data and analysis methods are described in Sect. 2. In Sect. 3, the structure of ENSO-associated wintertime teleconnection patterns in two PDO phases and synoptic-scale transient eddies feedbacks in terms of eddy-induced geopotential height tendencies are diagnosed. In addition, the atmospheric baroclinic growth environment along with the oceanic frontal zones is also investigated. The conclusion and discussion are presented in Sect. 4.

2 Data and methods

2.1 Data

The atmospheric data are obtained from the ERA-20C reanalysis data in the present study. As an outcome of the ERA-CLIM project, the ERA-20C is the first atmospheric reanalysis of the twentieth century from 1900–2010 by the European Centre for Medium-Range Weather Forecasts (ECMWF). The atmospheric general circulation model uses the same configuration as the control member of the ERA-20CM ensemble, forced by observational analyses of Hadley Centre Sea Ice and Sea Surface Temperature dataset (HadISST) version 2.1 for sea ice and SST, atmospheric composition changes, and solar forcing (Poli et al. 2016). The synoptic quality of the product and agreement in terms of climate indices with other products improve with the availability of observations. More information related to ERA-20C can be found on its webpage (<https://www.ecmwf.int/en/research/climate-reanalysis/era-20c>). Here the ERA-20C data covering 1950–2010 are used, since Chang and Yau (2016) have shown that the Pacific and Atlantic basin-wide transient eddy activities prior to 1950s derived from ERA-20C reanalysis dataset are unlikely to be reliable due to changes in density of surface observation, but the variations and trends after 1950 are consistent with those derived from independent observations.

The selection of strong ENSO episodes is adopted from NCEP/NOAA definition. It is based on a threshold of ± 0.8 °C for the Oceanic Nino Index (ONI) (3-month running mean of ERSST.v5 SST anomalies in the Nino-3.4 region), based on centered 30-year base periods updated every 5 years in order to remove a warming trend in the

Nino-3.4 region (more information about the strategy in NOAA website https://origin.cpc.ncep.noaa.gov/products/analysis_monitoring/ensostuff/ONI_change.shtml). In addition, the threshold is met for a minimum of five consecutive overlapping seasons including DJF (December–January–February). The PDO index used in the study is downloaded from the Joint Institute for the Study of the Atmosphere and Ocean Web site (<https://research.jisao.washington.edu/pdo/PDO.latest.txt>). It is the leading pattern (EOF) of monthly mean SSTA in the North Pacific basin (typically, poleward of 20° N). The monthly mean global average SSTA are removed to separate this pattern of variability from any “global warming” signal that may be present in the data. Since the PDO is a largely interdecadal oscillation, a 10-year low pass-filter is performed to highlight the interdecadal variations of PDO. This yields two periods with significant high PDO index values after 1950 (1978–1998 and 2002–2006) and three periods with low PDO index values (1950–1977, 1999–2001, and 2007–2010). They are agreeable with the decadal variation of PDO in Newman et al. (2016). Here the 1950 refers to the winter from the year 1950 to 1951. Following this definition, 23 strong ENSO winters (DJF, 69 months) are selected during the period 1950–2010, and sorted according to the two phases of PDO (Table 1). The monthly composites of variables for ENSO warm minus cold events will be shown first, and the composites highlight the linear component of ENSO response (Hoerling et al. 1997, 2001). One may thus argue that much is forfeited by analysis methods based on assumptions of linearity. So some discussions are made in the Conclusion and Discussion part about the asymmetry in the response to ENSO warm and cold events separately. When performing the composite analysis, all variables are detrended to remove the effect of global warming.

2.2 Methods

To extract the transient eddies associated with migratory synoptic-scale disturbances at periods of 2.5–6 days, a bandpass-filtered technique is applied to 6-hourly meridional wind (v) at 250 hPa. The transient eddy activities in the present study are measured with the variance of 2.5–6 days bandpass-filtered meridional wind at 250 hPa, by v^2 . The overbar represents averaging over a specified period, and the prime denotes perturbations with the period of 2.5–6 days.

Table 1 Classification of strong winter (DJF, 69 months) events based on the phases of ENSO and PDO for period of 1950–2010

1950.01–2010.12	PDO positive	PDO negative
ENSO warm	1982/83, 1986/87, 1987/88, 1991/92, 1997/98, 2002/03	1953/54, 1957/58, 1963/64, 1965/66, 1968/69, 1972/73, 2009/10
ENSO cold	1984/85, 1988/89, 1995/96, 1998/99	1955/56, 1970/71, 1973/74, 1975/76, 1999/2000, 2007/08

The midlatitude synoptic-scale transient eddy activities are believed to have their origin in processes encapsulated in the theory of baroclinic instability (Eady 1949; Hoskins and Valdes 1990). A suitable measure of the baroclinicity is provided by the Eady growth rate maximum:

$$\sigma_{Bl} = 0.31f \left| \frac{\partial \bar{v}_h}{\partial z} \right| / N \quad (1)$$

where f is the Coriolis parameter, \bar{v}_h is the monthly mean horizontal wind fields, and N is the Brunt–Väisälä frequency. Lindzen and Farrell (1980) have shown that this formula provides an accurate estimate of the growth rate maximum in a range of baroclinic instability problems.

The atmospheric response to thermal and dynamical forcing can be illustrated based on the following geopotential tendency equation that is derived from QGPV Equation (Lau and Holopainen 1984; Fang and Yang 2016):

$$\left(\frac{1}{f} \nabla^2 + \frac{f}{\sigma_1} \frac{\partial^2}{\partial p^2} \right) \left(\frac{\partial \bar{\Phi}}{\partial t} \right) = -f \frac{\partial}{\partial p} \left(\frac{\alpha}{\sigma_1} \frac{\bar{Q}_d}{T} \right) - f \frac{\partial}{\partial p} \left(\frac{\alpha}{\sigma_1} \frac{\bar{Q}_{eddy}}{T} \right) + \bar{F}_{eddy} + R_v, \quad (2)$$

where the overbar denotes the monthly mean in winter (DJF), $\frac{\partial \bar{\Phi}}{\partial t}$ is the initial geopotential tendency, R_v is a residual term including the horizontal advection of quasigeostrophic potential vorticity and friction, T is the temperature, f is the Coriolis parameter, σ_1 is the static stability parameter, and α is the specific volume. \bar{Q}_d is the monthly mean diabatic heating that can be diagnosed as a residual of the thermodynamic equation, \bar{Q}_{eddy} is the monthly mean transient eddies heating, \bar{F}_{eddy} is the transient eddies vorticity feedback (or forcing) that is determined by the convergence of vorticity flux transport, $\bar{F}_{eddy} = -\nabla \cdot \bar{v}_h \zeta'$, where ζ' is the relative vorticity, \bar{v}_h is the horizontal wind vector, the prime denoted the transient eddies (2.5–6 days bandpass).

It can be found that the atmospheric potential vorticity source can be mainly generated by three terms on the right side of Eq. (2): diabatic heating, transient eddy heating, and transient eddy vorticity feedbacks. The first term is direct thermal forcing by diabatic heating, which is relatively weak in the midlatitude and usually creates the baroclinic structure of atmospheric circulation anomaly confined below the middle troposphere in the vertical direction (Fang and Yang 2016). The last two terms are associated with transient eddies, and it will be positive (negative) if there is a convergence (divergence) of eddy vorticity flux within a certain region. The role of transient eddy vorticity feedbacks will be focused on in the present study.

In addition, to examine the effect of ENSO-associated SSTA in two PDO phases on atmospheric teleconnection patterns, three idealized numerical experiments have

been performed using Version 4.0 of the Community Atmosphere Model developed by the National Center for Atmospheric Research (CAM4.0) with horizontal resolution T42 (64×128), which has been widely used in climate simulation (Neale et al. 2010; Gent et al. 2011; Jiang et al. 2019). A control experiment is forced by winter mean SST for 1950–2010 which are taken from the HadISST dataset. Two sensitivity experiments, named SSTA_ENSO@PDO+ and SSTA_ENSO@PDO- simulations, are designed with the winter mean SST added to idealized SSTA in a specific region of tropical Pacific–Indian Ocean and North Pacific (bounded by 40° E– 290° E, 20° S– 70° N). For SSTA_ENSO@PDO+ simulations, the idealized SSTA is derived from the composite of SST anomalies for ENSO warm minus cold events in the PDO positive phase shown in Fig. 1a. While for SSTA_ENSO@PDO- simulations, the idealized SSTA is derived as that in PDO negative phase shown in Fig. 1b. Each of these three runs is initiated from the same sea ice and atmospheric conditions, and integrated for 20 years. Assuming that each year is statistically independent, this is equivalent for the anomaly experiments to an ensemble mean with 20 realizations.

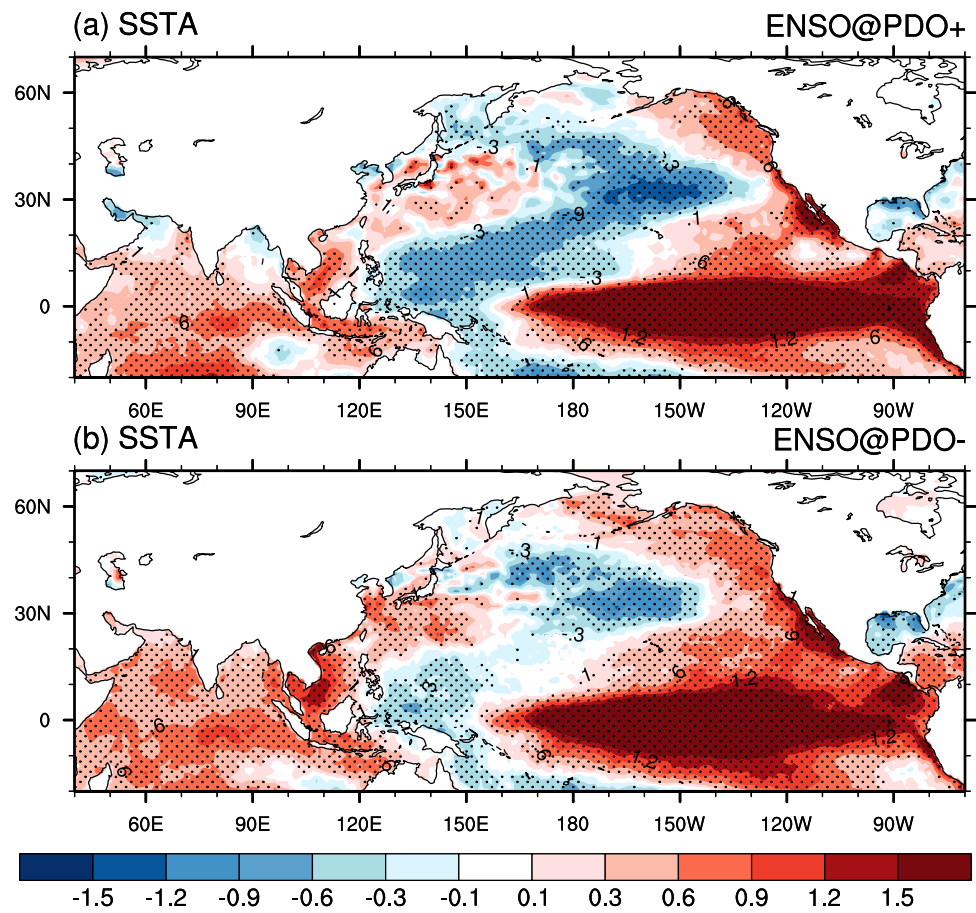
3 Results

3.1 ENSO-associated atmospheric teleconnections in two PDO phases

Composites of SST anomalies for ENSO warm minus cold events in PDO positive and negative phase is shown in Fig. 1. The most pronounced feature in PDO positive phase is positive anomalies in tropical central-eastern Pacific and extending poleward along the eastern boundary, positive anomalies in tropical Indian Ocean, and opposite anomalies in tropical western Pacific and North Pacific (Fig. 1a). Similar positive anomalies in tropical central-eastern Pacific and tropical Indian Ocean, but the SSTA in the rest of Pacific present different in PDO negative phase (Fig. 1b). The SST negative anomalies in tropical western Pacific and midlatitude North Pacific behave much warmer in PDO negative phase, while seeming colder in PDO positive phase.

Composites of geopotential height anomalies at 300 hPa for all ENSO warm minus cold events in the PDO positive and negative phase are displayed separately in Fig. 2. A positive phase of PNA pattern is observed with a large negative anomaly over midlatitude Northeast Pacific, a positive anomaly over northern North America, and a relatively weak negative anomaly over southern United States (Fig. 2a, red

Fig. 1 Composites of sea surface temperature anomalies (SSTA, unit: K) for ENSO warm minus cold events in **a** PDO positive and **b** negative phase for winter of 1950–2010. Hatched areas are statistically significant at the 5% level based on the Student's *t* test

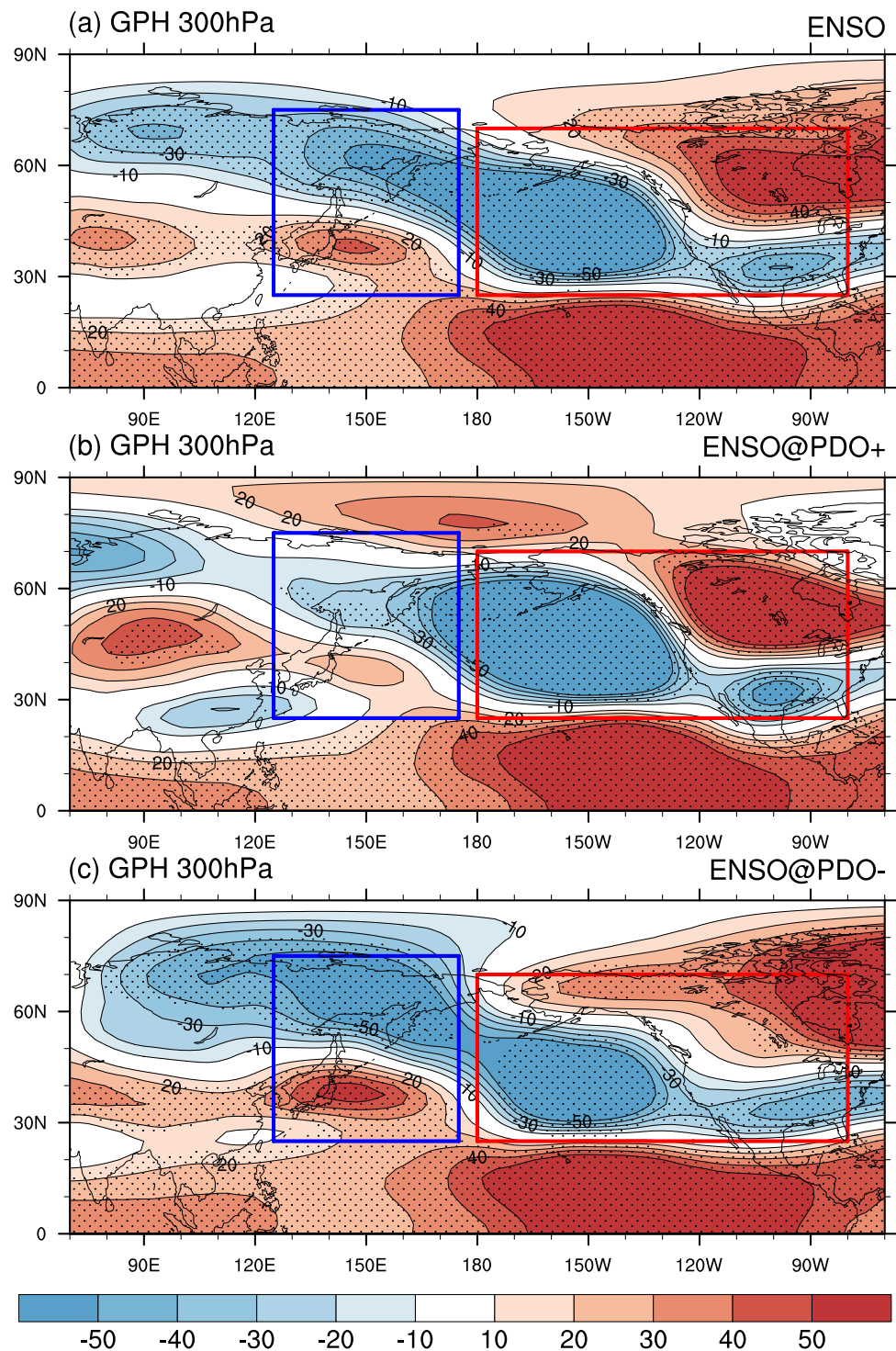


box), which is strongly influenced by ENSO warm events. In PDO positive phase, the PNA pattern is significantly strengthened with all enhanced centers (Fig. 2b, red box). However, in PDO negative phase the PNA pattern presents less robust, with a weak negative anomaly over Northeastern Pacific, and a weak dipole centers over North America, except with a slight downstream shift (Fig. 2c, red box). The other noteworthy feature in PDO negative phase is the negative phase of WP pattern characterized by north–south dipolar centers over the Far East (Fig. 2c, blue box), but does not present in PDO positive phase.

The vertical structures of composites of geopotential height anomalies are shown in Fig. 3. The main center of WP and PNA pattern for latitude-average is between 140°E – 160°E and 140°W – 160°W , respectively. The PDO positive phase is characterized by a relatively strong baroclinic signature with diabatic heating influence in the tropics, which demonstrates tropical convection associated with tropical Pacific SSTA plays a critical role in the response, while the midlatitude negative anomaly of strengthened PNA pattern exhibits equivalent barotropic structure (Fig. 3a). In comparison, in PDO negative phase the tropical positive anomaly seems similar, but the

midlatitude negative anomaly of less-robust PNA pattern appears to be a slender range (Fig. 3b). To the WP pattern over the Far East, the vertical structure is relatively weak in PDO positive phase (Fig. 3c), but impressive in PDO negative phase (Fig. 3d). The negative anomaly over middle-to-high latitude suggests characteristic eddy-driven equivalent barotropic structure, while the positive anomaly northward phase tilt with height may be involved in both transient eddies feedback and diabatic heating influence. Accompanying with the atmospheric teleconnections, the vertical structure of composites of zonal wind anomalies and the climatology (jet stream) are shown in Fig. 4. The midlatitude south-positive north-negative dipole anomalies of zonal wind perform exactly consistent with the strengthened PNA pattern over Northeast Pacific in PDO positive phase (Fig. 4a). In PDO negative phase, similar but slender dipole anomalies of zonal wind are also observed accompanying with the less-robust PNA pattern over there (Fig. 4b). However, the zonal wind anomalies associated with the WP pattern are significantly strengthened over the north side of the climatological main body of jet in PDO negative phase (Fig. 4d), but rather feeble in PDO positive phase (Fig. 4c).

Fig. 2 Composites of geopotential height anomalies at 300 hPa (GPH, unit: m) for **a** all ENSO warm minus cold events, and ENSO warm minus cold events in **b** PDO positive and **c** negative phase for winter of 1950–2010. Stippled areas are statistically significant at the 5% level based on the Student's *t* test



3.2 The transient eddy feedbacks to teleconnections

The strength of transient eddy activities is usually strongest at the level of 300 hPa from its vertical structure (Han et al. 2007). Here, the climatology of statistical transient eddy

activities (black contour) and Pacific jet stream main body (blue contour) at 300 hPa are shown in Fig. 5. It displays that the maximum of transient eddy activities presents near the exit region of jet stream and extends downstream. Composites of transient eddy activities anomalies for ENSO warm minus cold events in PDO positive and negative phase are

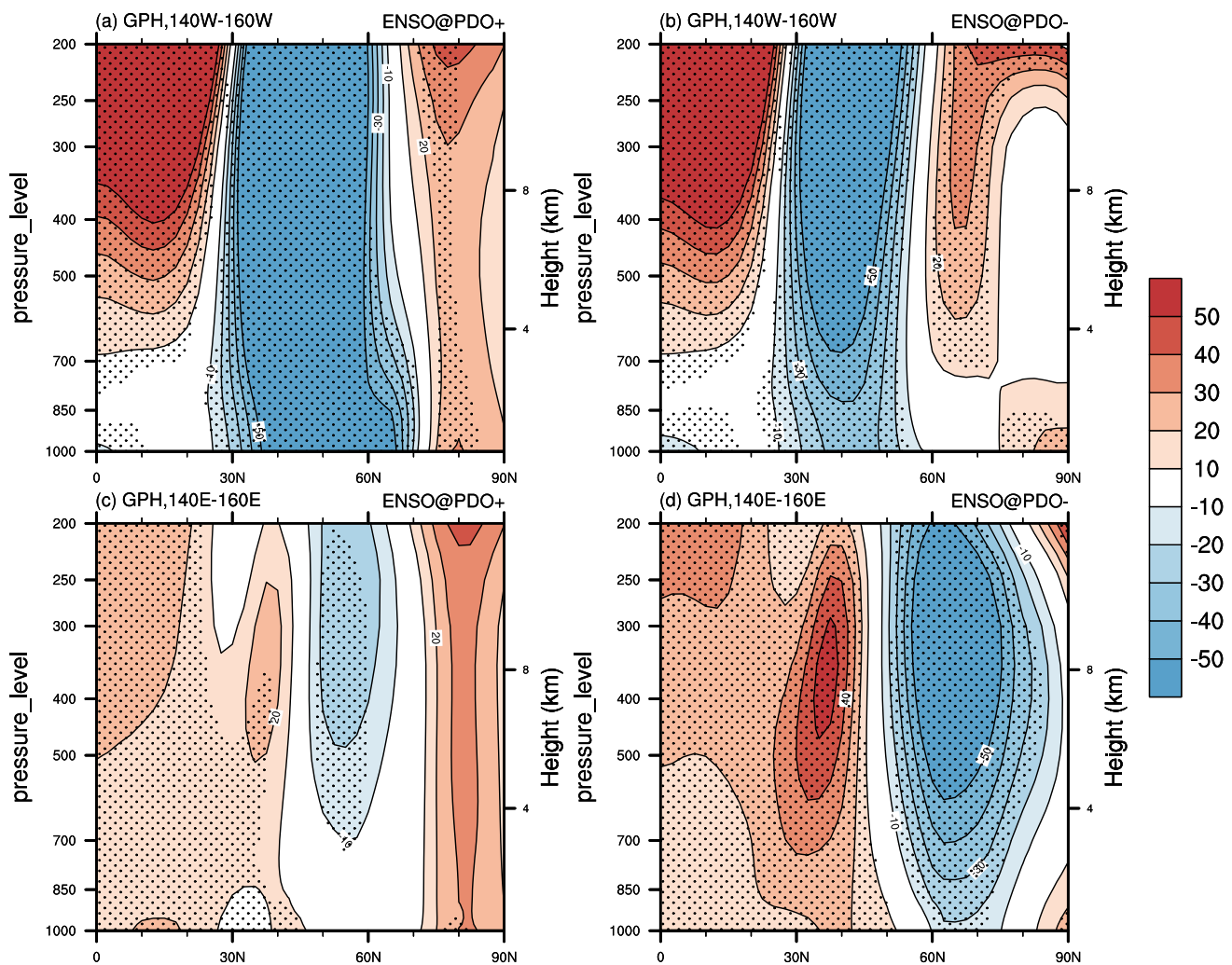


Fig. 3 Latitude-altitude sections of composites of geopotential height anomalies (GPH, unit: m) for ENSO warm minus cold events in **a, c** PDO positive and **b, d** negative phase for winter of 1950–2010. Stippled areas are statistically significant at the 10% level based on the Student's *t* test

also demonstrated. In PDO positive phase, positive anomalies of Pacific transient eddy activities generally exhibit uniform equatorward and downstream, through midlatitude eastern Pacific, and extend to southern North America (Fig. 5a). In PDO negative phase, the equatorward and downstream anomalies over midlatitude eastern Pacific are somewhat less powerful than what is found in PDO positive phase, and relatively non-uniform. Meanwhile, remarkably strengthened anomalies occur over the north side of the climatological entrance of the storm track (Fig. 5b). It is coordinated with the upstream intensified westerly jet anomalies in Fig. 4d.

The transient eddy activities influence mean flow through the convergence of eddy momentum and heat fluxes and provide a forcing on mean flow (Lau and Nath 1991; Chang and Fu 2002; Ren et al. 2008). The transient

eddy forcing is recognized as important for understanding the generation and maintenance of mean flow anomalies. The transient eddies can redistribute momentum and heat in the atmosphere, and thus can induce and maintain general circulation anomalies (e.g., Lau and Holopainen 1984; Fang and Yang 2016). Previous studies have demonstrated the dynamical interactions between transient eddies and low frequency variation, which provide the quantitative estimate of the effect (e.g., Lorenz and Hartmann 2001, 2003). Here, the transient eddy vorticity forcing is illustrated per Eq. (2). The composites of geopotential tendencies anomalies at 300 hPa induced by transient eddy vorticity forcing for ENSO warm minus cold events in PDO positive and negative phase are shown in Fig. 6, and the vertical structures in Fig. 7. In PDO positive phase, the striking feature is geopotential height tendency negative

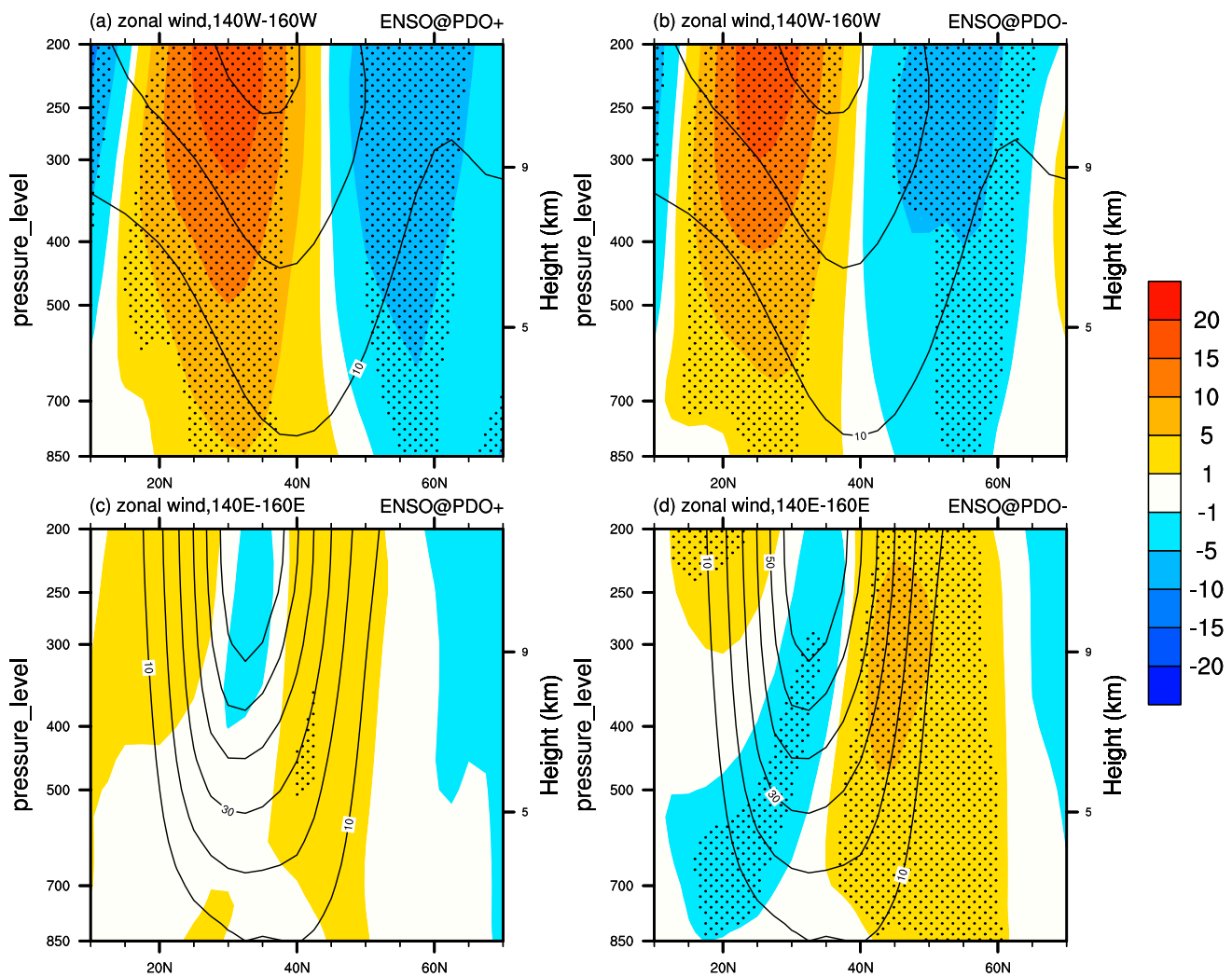


Fig. 4 As in Fig. 3, but for the zonal wind anomalies

anomalies over Northeastern Pacific (Fig. 6a). From its vertical structure in Fig. 7a, the negative anomalies appear typical eddy-driven characteristics as an equivalent barotropic structure in middle-upper troposphere, which is consistent with the observation in Fig. 3a. That suggests the negative height tendency anomalies are largely in favor to the observed negative anomalies of the strengthened PNA pattern over the Northeastern Pacific (Fig. 2b). We also notice that positive geopotential tendency anomalies over the south to the Kamchatka peninsula in Fig. 6a are not well consistent with that in Fig. 2b. Combined with the transient eddy anomalies shown in Fig. 5a, the positive anomalies may be associated with negative transient eddy anomalies over high latitude. In PDO negative phase, the negative geopotential tendency anomalies over Northeastern Pacific still present, but the strength is less powerful (Fig. 6b). From its vertical structure, it also displays the

equivalent barotropic structure of eddy-forcing, but slightly weaker than that in PDO positive phase (Fig. 7b). The noteworthy feature of height tendency anomalies in PDO negative phase is large-scale negative anomalies over the Far East, which is centered over near the Kamchatka Peninsula (Fig. 6b). From its vertical structure, it performs a typical eddy-driven structure almost through the entire troposphere (Fig. 7d). It is coincident with the observed WP negative pattern in Fig. 2, suggesting the anomalies greatly favor the observed negative WP pattern. To the positive anomalies on its south flank, its vertical structure coincides with the south branch of the observed WP pattern.

The midlatitude transient eddy activities are primarily attributed to the atmospheric baroclinicity. Eady growth rate maximum is an accurate measure of the atmospheric baroclinicity (Hoskins and Valdes 1990). Since the baroclinic development primarily occurs in the lower troposphere,

Fig. 5 Composites of transient eddy activities anomalies at 300 hPa (unit: m^2/s^2 , shaded) for ENSO warm minus cold events in **a** PDO positive and **b** negative phase, and its climatology (black contoured from 100 to 150 by 50 m^2/s^2) and the climatology of westerly jet at 300 hPa (blue contoured from 40 to 60 by 20 m/s) for winter of 1950–2010. Stippled areas are statistically significant at the 5% level based on the Student's *t* test

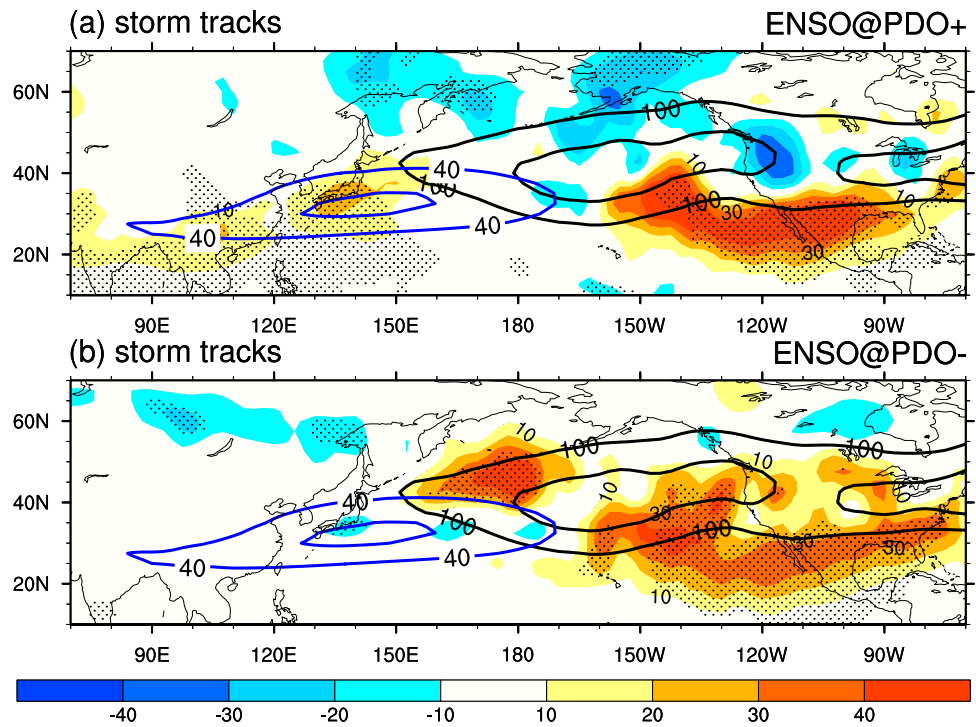
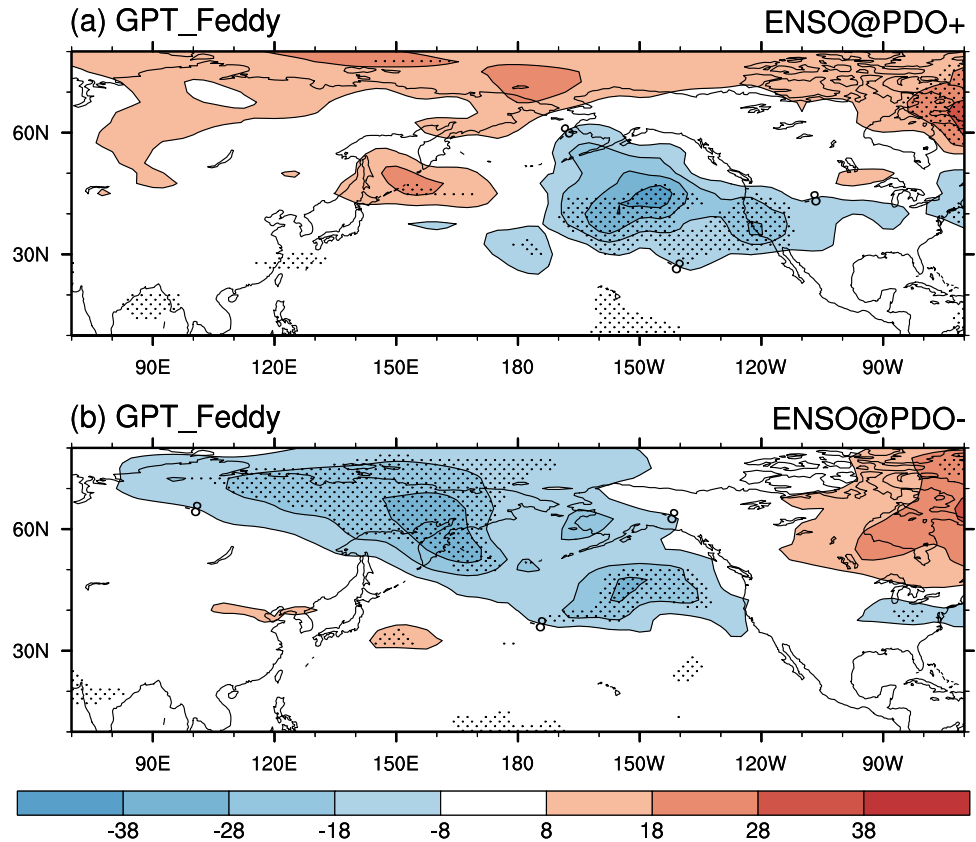


Fig. 6 As in Fig. 5, but for the geopotential tendencies anomalies at 300 hPa ($10^{-4} m^2 s^{-3}$) induced by transient eddy vorticity forcing. Stippled areas are statistically significant at the 5% level based on the Student's *t* test



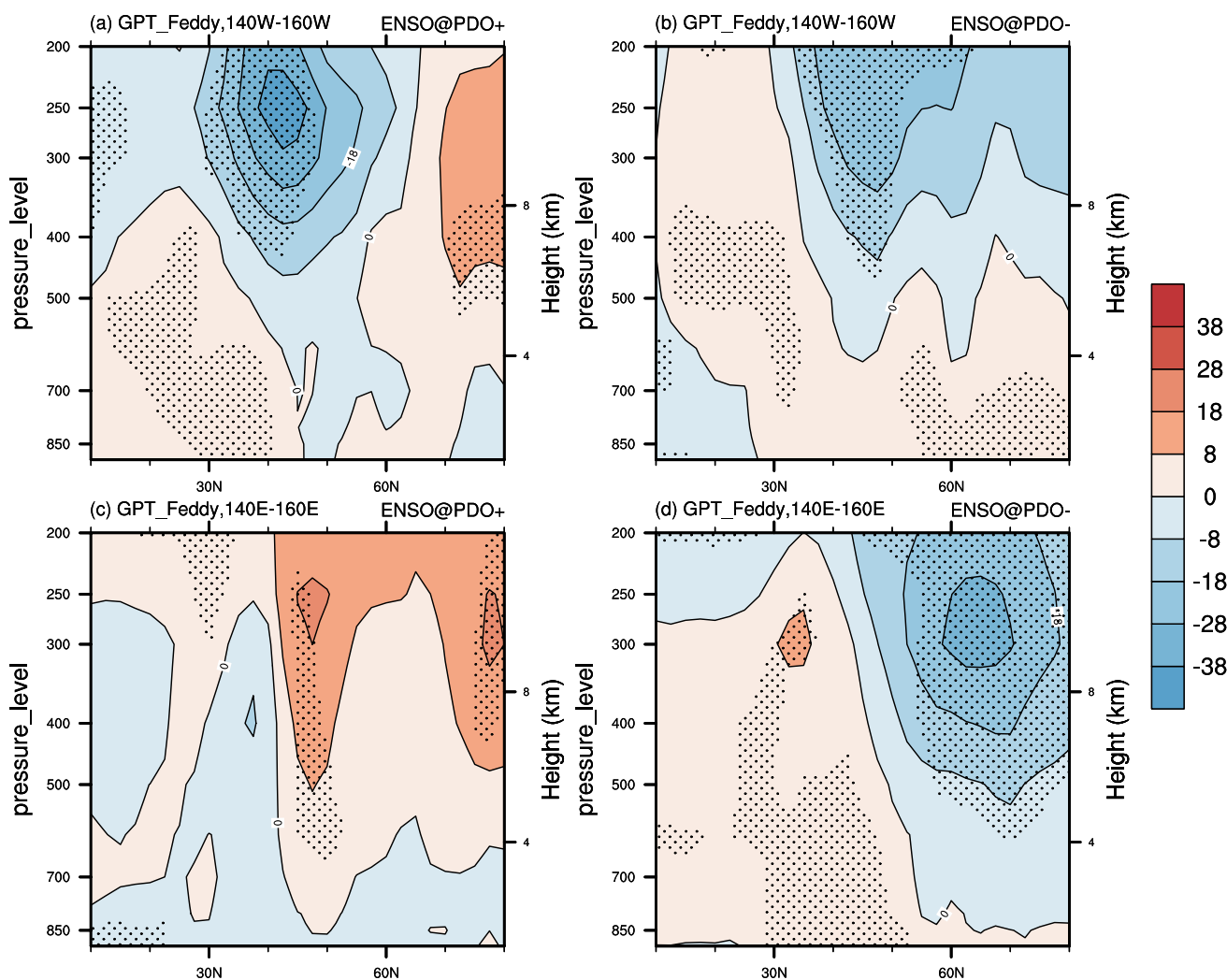


Fig. 7 As in Fig. 3, but for geopotential tendencies anomalies ($10^{-4} \text{ m}^2 \text{ s}^{-3}$) induced by transient eddy vorticity forcing. Stippled areas are statistically significant at the 10% level based on the Student's t test

the climatology and composites of growth rate maximum anomalies between 900 and 800 hPa for ENSO warm minus cold events in PDO positive and negative phase are shown in Fig. 8a, b. The climatological distribution of growth rate (black contour) displays that the maximum of baroclinicity generally presents in the same location of jet stream. In PDO negative phase (Fig. 8b, blue box), the poleward positive anomalies over the Far East and the extension are more remarkable than what is found in PDO positive phase (Fig. 8a) and relatively uniform. It offers baroclinic instability to the generation of downstream strengthened transient eddy anomalies shown in Fig. 5b. The baroclinicity is mainly determined by the vertical wind shear and the Brunt–Väisälä frequency mentioned in Eq. (1). In contrast to the small anomaly of winter Brunt–Väisälä frequency over there, the corresponding vertical wind shear anomalies in

PDO negative phase (Fig. 8d) are responsible for the growth rate anomalies shown in Fig. 8b.

3.3 The possible connection of subarctic frontal zones

The above section highlights the atmospheric internal dynamics of PNA/WP patterns from the perspective of transient eddy feedbacks. It suggests that vorticity feedback from synoptic-scale transient eddies can greatly benefit to the maintenance of the PNA/WP patterns. In this section, we will extend the study to investigate the possible connection between oceanic frontal zones and the transient eddies from the perspective of local air–sea interaction. Figure 9 shows composites of wind stress and wind stress curl anomalies for ENSO warm minus cold events in both positive and negative

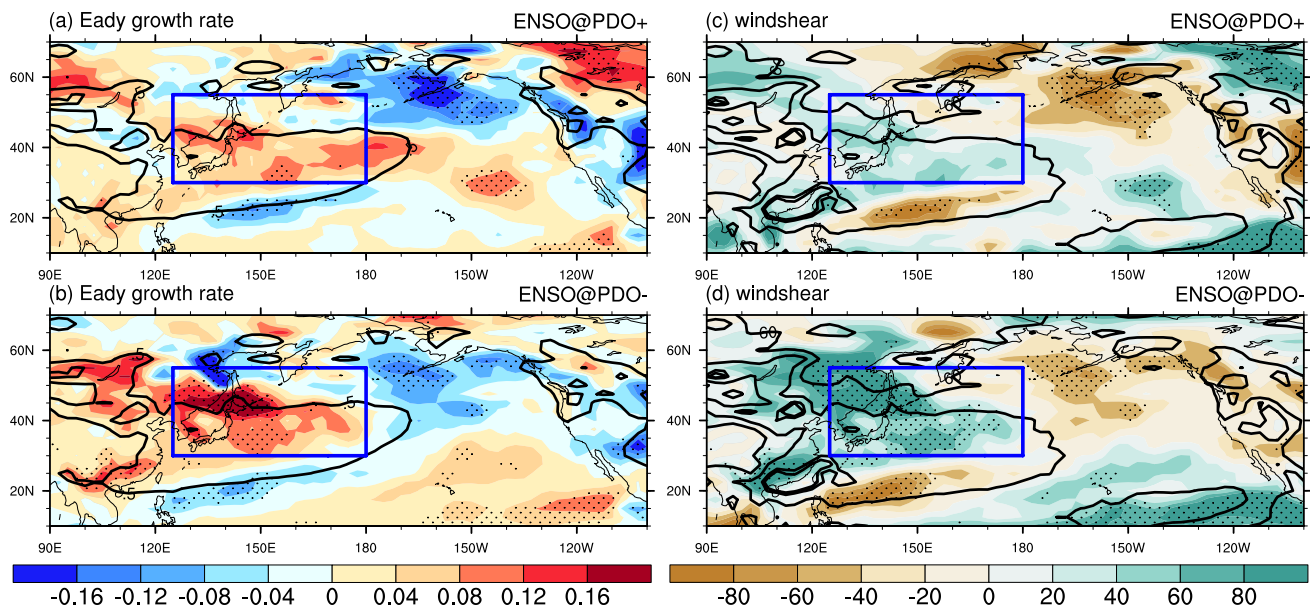


Fig. 8 Composites of **a, b** the growth rate maximum (unit: day^{-1} , shaded) and **c, d** the vertical wind shear anomalies between 900 and 800 hPa (unit: day^{-1} , shaded) for ENSO warm minus cold events in **a, c** PDO positive and **b, d** negative phase for winter of 1950–2010,

and the climatology (growth rate maximum contoured from 0.5 to 1.5 by 0.5 day^{-1} and vertical wind shear contoured from 60 to 500 by 200 day^{-1}), respectively. Stippled areas are statistically significant at the 5% level based on the Student's t test

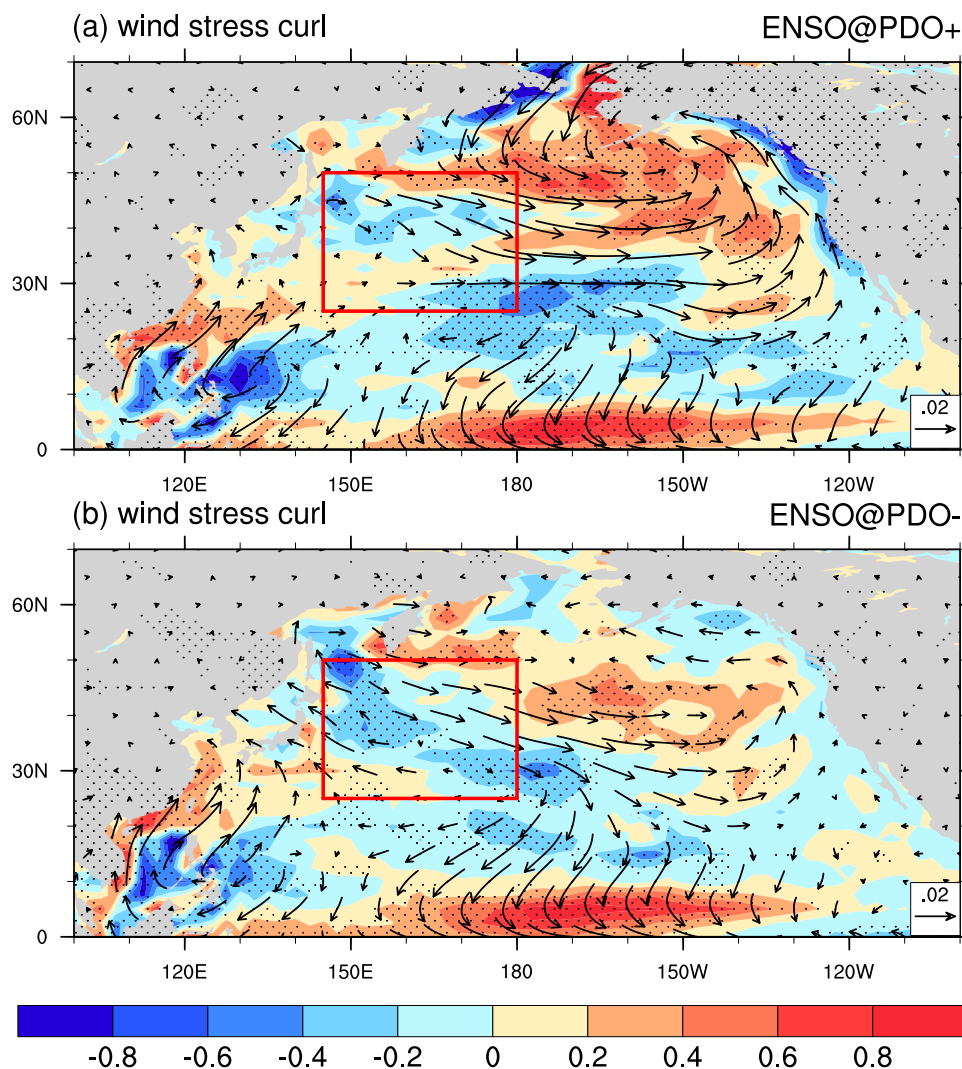
PDO phases. In PDO positive phase (Fig. 9a), large-scale strengthened cyclonic surface wind stress curl anomalies occupy Northeast Pacific. Because of the cyclonic anomalies, the anomalous intensified surface westerly increases the upward heat flux and cool the ocean. The intensified westerly could also drive a southward Ekman cold advection, eventually lead to the negative SSTA and enhance the SST gradient in the Northeastern Pacific shown in Fig. 1a. However, in PDO negative phase (Fig. 9b), the cyclonic curl anomalies seem less strengthened accompanying with relatively weak SSTA in the Northeastern Pacific (Fig. 1b). It is remarkable that anticyclonic anomalies of wind stress curl accompanying with a southeast wind at the south part exist over Northwestern Pacific in this situation (Fig. 9b, red box). The anomalous southerly strengthens downward surface heat flux over the southeast to Japan. The corresponding Ekman advection and downward Ekman pumping transport warm water and generate positive SSTA (Fig. 1b).

In condition of such wind stress and SST anomalies, Fig. 10 shows the climatological distribution of wintertime SST meridional gradient and the composites in PDO positive and negative phase. The climatological distribution demonstrates that two major zones of tight SST gradients locate in the middle Northwest Pacific, commonly named SAFZ near 42°N (contour, Fig. 10a, b), and STFZ around 28°N , merge in Northeast Pacific. The SAFZ front with a strong SST gradient associated with western boundary currents and their extensions is usually much stronger than STFZ,

also demonstrated in the climatology zonally-averaged over 145°E – 180°E (Fig. 10c, black curve). In PDO negative phase, the center of SAFZ appears overall enhancement and somewhat northward shift, meanwhile the gap between two frontal zones weakens (Fig. 10b). It is more obvious from the zonally-averaged distribution (Fig. 10c, red curve), calculated by the zonally-averaged climatology adding the anomalies for ENSO events in PDO negative phase. However, the SAFZ performs overall decrease, but STFZ seems intensified in PDO positive phase both from the horizontal distribution (Fig. 10a) and zonally-averaged distribution (Fig. 10c, blue curve).

Previous studies suggest a potential importance of the oceanic frontal zones with pronounced SST gradient, which mainly respond to the basin-scale wind stress (Kwon et al. 2010), on anchoring and maintaining atmospheric surface baroclinicity, energizing transients eddy activities, and jet stream from observation and atmospheric general circulation model experiments (Nakamura et al. 2004; Xu et al. 2011; Yao et al. 2016). Major transient eddy activities and associated polar-front jet are organized along or just downstream of major oceanic frontal zones from observation (Nakamura et al. 2004, 2008). Figure 11a shows the climatology of latitude-altitude sections of growth rate maximum (contour) and composite anomalies in PDO negative phase (shade). It can be found that positive anomalies of atmospheric baroclinicity strengthen on the north side of the climatological main body in the low-to-middle troposphere,

Fig. 9 As in Fig. 6, but for wind stress (unit: N m^{-2} , vector) and curl anomalies (unit: $\text{N m}^{-2} (10^4 \text{ km})^{-1}$, shaded). Stippled areas are statistically significant at the 5% level based on the Student's t test

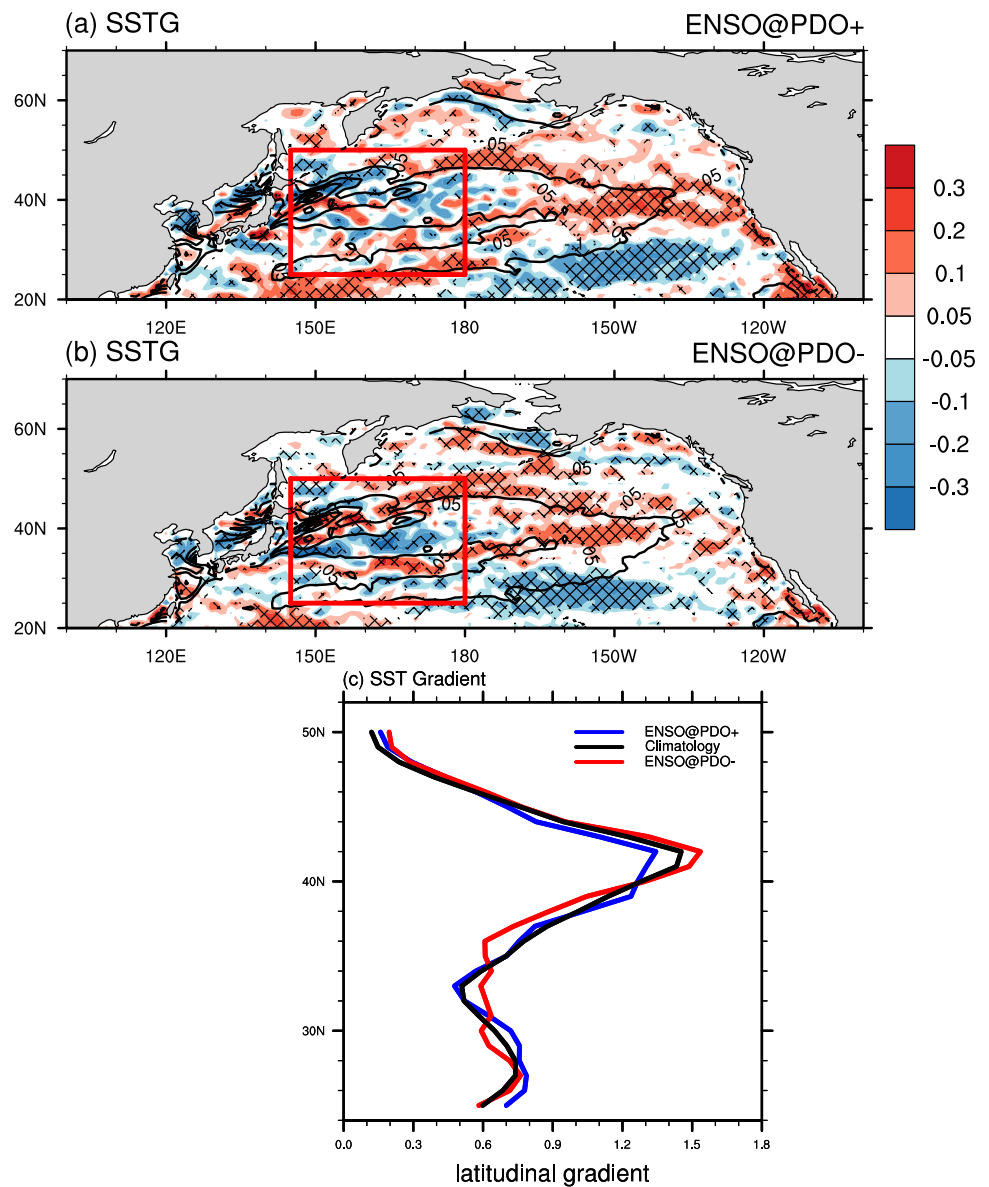


which is just overlying the enhanced and northward shifting SAFZ (Fig. 10b). The climatology of downstream transient eddy activities and the composite anomalies in PDO negative phase are shown in Fig. 11b. The transient eddy anomalies strengthen over the north side of its climatological main body, which is just above the strengthened atmospheric baroclinicity anomalies. It may suggest the possible anchor effect of the strengthened SAFZ in Northwest Pacific to maintain atmospheric lower baroclinicity anomalies, and energize transient eddy anomalies from the view of baroclinic generation. The transient eddy anomalies, which may be mainly induced by baroclinic generation, contribute a lot in shaping the WP pattern in PDO negative phase. However, in PDO positive phase, the vertical atmospheric baroclinicity anomalies perform no significant enhancement over there, consistent with the horizontal distribution of growth rate maximum anomalies in Fig. 8a. In consequence, the transient eddy activities manifest no change.

4 Conclusion and discussion

The ENSO-associated wintertime atmospheric teleconnection patterns in two Pacific Decadal Oscillation (PDO) phases are obtained based on the ERA-20C reanalysis data during the period of 1950–2010. Different features of the teleconnection behavior are captured when ENSO events occur in different PDO phases. A strengthened ENSO-associated Pacific-North America (PNA) pattern presents in PDO positive phase, while a typical West Pacific (WP) pattern over Far East and a squeezed PNA pattern coexist when ENSO events occur in PDO negative phase. The midlatitude teleconnections generally exhibit eddy-induced equivalent barotropic structure in the vertical direction. The dynamical role of atmospheric midlatitude transient eddy feedbacks to the teleconnection patterns, and the possible coupled relationship between atmospheric transient eddy anomalies and

Fig. 10 **a, b** As in Fig. 1, but for the SST meridional gradient anomalies (SSTG, unit: K/100 km, shaded), and its climatology (contoured from 1 to 3 by 1 K/100 km). Stippled areas are statistically significant at the 5% level based on the Student's *t* test. **c** Climatological SSTG zonally-averaged over 145° E–180° E (black curve), and mean state for ENSO events in PDO positive (blue curve) and negative phase (red curve)



subarctic oceanic frontal zones (SAFZ) for maintaining the WP pattern are highlighted in the present study.

When ENSO events occur in PDO positive phase, the uniform strengthened westerly jet anomalies downstream of the main body of jet accompany with energetic transient eddy anomalies over Northeastern Pacific. The corresponding transient eddy anomalies shift downstream and equatorward, and the feedbacks largely enhance and favor the strengthened PNA pattern. When ENSO events occur in PDO negative phase, the strengthened westerly jet anomalies appear to split into two parts. One locates at the north side of the climatological main body of jet over Northwest Pacific, and the

other locates at the downstream of jet over Northeast Pacific. In this situation, the downstream transient eddy anomalies weaken, and the feedbacks reduce and form a relatively weak PNA pattern. However, the transient eddy anomalies over Northwest Pacific strengthen accompanying with the poleward strengthened SAFZ. The strengthened SAFZ could maintain the low-to-middle atmospheric baroclinicity anomalies, thus sustain the transient eddy anomalies. Then the transient eddy anomalies give feedback and distribute the atmospheric circulation, and outstandingly contribute to the WP teleconnection pattern over the Far East.

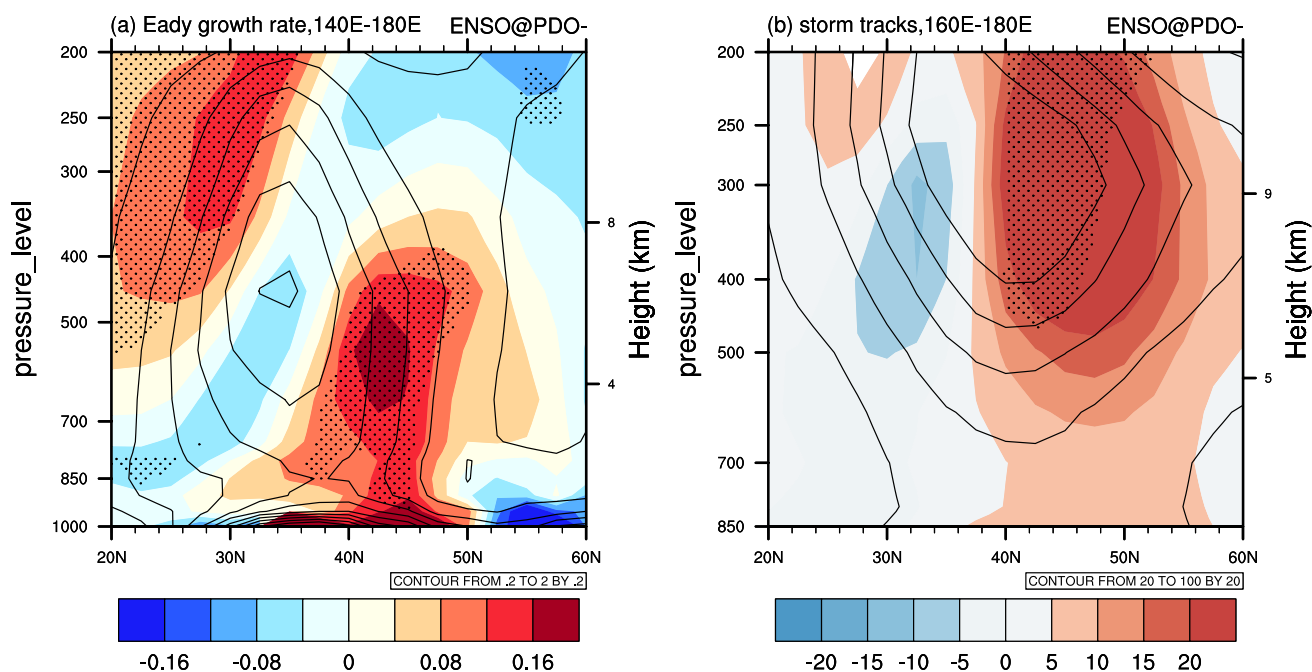


Fig. 11 Latitude-altitude sections of composites of **a** the growth rate maximum (shade, unit: day^{-1}) and **b** the transient eddy activities anomalies (shade, unit: m^2/s^2) for ENSO warm minus cold events in

PDO negative phase, and climatology (contour) for winter of 1950–2010. Stippled areas are statistically significant at the 10% level based on the Student's *t* test

In the present study, the dynamical role of atmospheric midlatitude atmospheric transient eddy feedbacks to the ENSO-associated wintertime teleconnection patterns in two PDO phases is highlighted without evaluating the ENSO independent variability of the PDO. Both ENSO and PDO are not a single dependent phenomenon, but instead the result of the combination of different physical processes, including oceanic wave variability and atmosphere–ocean interaction, which operate and generate effects on different time scales. However, an instructive method (Chen et al. 2013) is applied to objectively evaluate ENSO independent variability of PDO. The PDO-related part is calculated by linear regression of Nino-3.4 index with respect to winter PDO index, which is called PDO-related ENSO. Then the PDO-unrelated part is calculated as the difference between the total Nino-3.4 index and the PDO-related part. Considering PDO has both interannual and interdecadal variability, one is the interannual-PDO regression method, and the other is the interdecadal-PDO regression method. The interannual-PDO-related part is calculated by linear regression of Nino-3.4 index with respect to the interannual PDO index. Then the PDO-unrelated part is computed as the

difference between the Nino-3.4 index and the interannual-PDO-related part. The corresponding indexes are shown in Fig. 12a. To most ENSO extreme cases, they are still eligible for the selection criteria. However, four events, 1986/87, 1987/88, 2002/03, 2007/08 are out. In this situation, only three events are left for ENSO warm events in PDO positive phase. That means the statistical test will be affected. The other is the interdecadal-PDO regression method. Since the PDO emphasizes the interdecadal variability, a 10-year low pass-filter is performed to highlight the interdecadal variations of PDO, named interdecadal PDO index. The interdecadal-PDO-related part is calculated by linear regression of Nino-3.4 index with respect to the interdecadal PDO index. Then the PDO-unrelated part is computed as the difference between the Nino-3.4 index and the interdecadal-PDO-related part. The corresponding indexes are shown in Fig. 12b. In this situation, we find that the 22 ENSO extreme events still exist, except 1987/88. That means the results will generally not be affected. Moreover, a 10-year high pass Butterworth filter is applied to the corresponding variables in order to remove above 10-year timescales interdecadal component, mostly removing PDO effect.

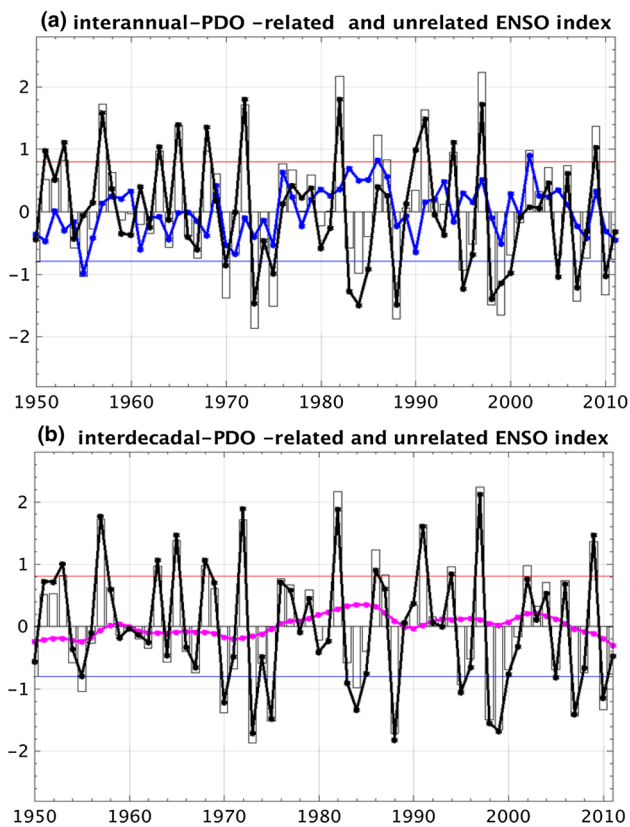


Fig. 12 Time series of normalized Niño-3.4 index for winter of 1950/51–2009/10 (bar). **a** The interannual-PDO-related part (blue curve), and the interannual-PDO-unrelated part of Niño-3.4 index (black curve), **b** the interdecadal-PDO-related part (purple curve), and the interdecadal-PDO-unrelated part of Niño-3.4 index (black curve)

The results are highly consistent with the present results. We consider that linear interdecadal component may be mostly cancelled out in the subtraction of El Niño minus La Niña whether in PDO positive or negative phase. The remaining difference in PDO positive/negative phase may be mainly obtained from nonlinear modulation of PDO phase on ENSO effect.

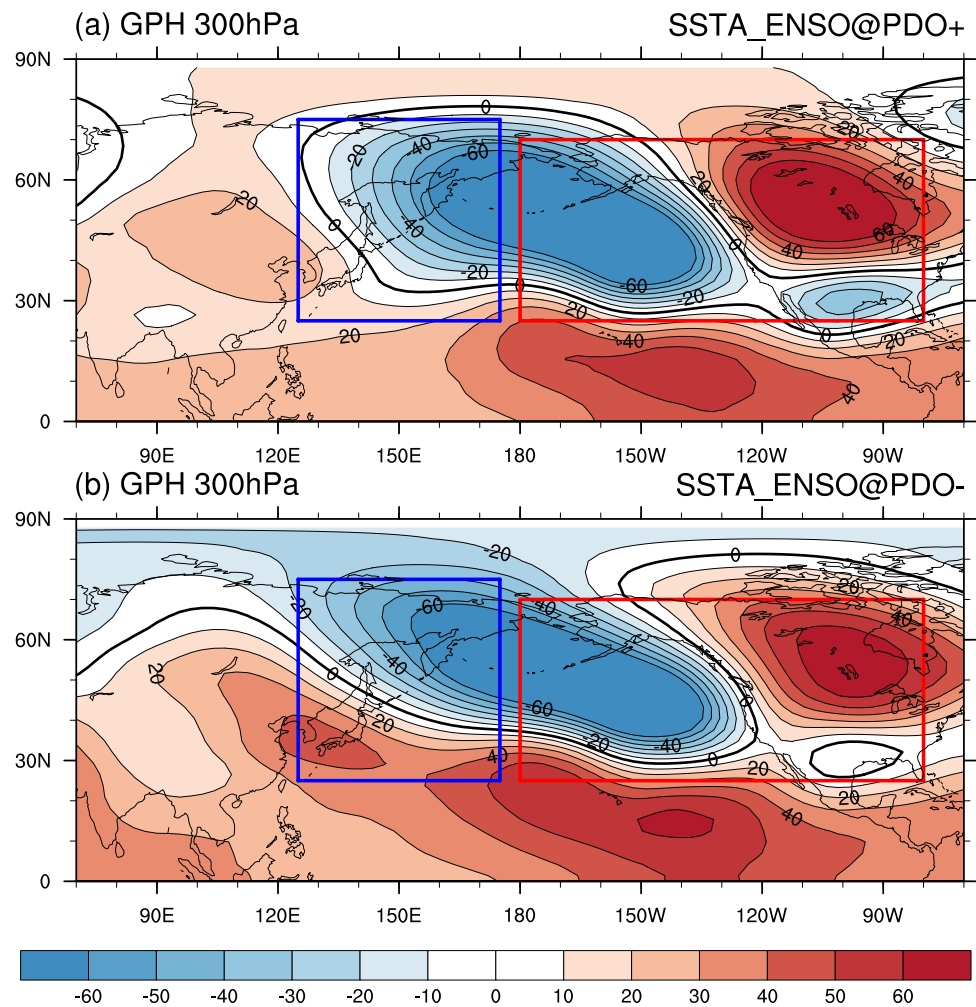
To examine the effect of the ENSO-associated SSTA in two PDO phases on the atmospheric teleconnection patterns, two sensitivity SSTA experiments have been performed. The simulated results shown in Fig. 13 demonstrate that the corresponding SSTA experiments generally reproduce the observed teleconnection patterns, a strengthened PNA pattern in SSTA_ENSO@PDO+ experiment and a WP and less-robust PNA patterns coexisting in SSTA_ENSO@PDO- experiment. It suggests that the teleconnection patterns primarily

originate from the ENSO-associated SSTA patterns in two PDO phases. Comparing the observation, the WP pattern in model results seems similar strength with a little tilting (Fig. 13b). That may be due to the model experiments are only conducted in specific region with idealized SSTA, but other factors, such as North Atlantic SSTA, polar sea ice, even upper wave propagation (Chen et al. 2005) that could affect atmospheric teleconnections are not involved.

Given the asymmetric atmospheric response to ENSO warm and cold events, the attribution of ENSO-associated teleconnections is detected by dividing ENSO events into four categories according to PDO phases. The asymmetric SSTA of ENSO warm and cold events in PDO positive or negative phase have been shown in Fig. 14. In PDO positive phase, the SSTA in El Niño events performs not exactly inverse, but the amplitude is stronger than that in La Niña events, especially in North Pacific (compare the upper two panels, Fig. 14a, b). In PDO negative phase, the SSTA in La Niña events performs stronger than that in El Niño events (compare the below two panels, Fig. 14c, d). That means the SSTA performs asymmetric in El Niño and La Niña whether in PDO positive and negative phases. Under the different SSTA conditions, the geopotential height anomalies also exhibit different features in four phases. In PDO positive phase, a typical strengthened El Niño-associated PNA positive pattern occupies over North Pacific and North America (Fig. 14e), while a relative weak PNA negative pattern occurs in La Niña events (Fig. 14f). In PDO negative phase, a distinguished WP negative pattern with dipole centers over the Far East and weak PNA positive pattern coexists in El Niño events (Fig. 14g), while only PNA-like negative pattern appears in La Niña events (Fig. 14h).

The variability of midlatitude SST and oceanic frontal zones driven by basin-scale wind stress anomalies has been diagnosed. The results are consistent with the previous studies that the midlatitude low-frequency SST variability is primarily driven by basin-scale wind stress curl variability (Kwon et al. 2010). However, due to the lack of ocean variability in ERA-20C reanalysis data, the oceanic Rossby wave adjustment of gyre-scale circulation which may modulate the latitude and strength of the oceanic front cannot be demonstrated. While this work extends our understanding of dynamical relationship between ENSO-associated atmospheric patterns and transient eddy feedbacks in two PDO phases, the possible air–sea coupled connection between oceanic frontal zones and the transient eddy anomalies is also involved without the detail process from oceanic frontal zones through atmospheric boundary layer to free atmosphere. Nakamura et al. (2008) explored the importance of

Fig. 13 Composites of geopotential height anomalies at 300 hPa (GPH, unit: m) induced by idealized SSTA in specific region shown in Fig. 1 using CAM4.0/NCAR



the frontal zone for the intensity and structure of annular mode with a pair of high-resolution (~ 150 km) AGCM experiments through examining turbulent sensible and latent heat fluxes from the sea surface. Minobe et al. (2008) revealed that the Gulf Stream affects entire troposphere in a systematic manner, from surface to tropopause, and pointed out that the oceanic front enhanced latent and sensible heating plays a fundamental role in shaping tropospheric general circulation, using high-resolution observations and AGCM

experiments. In the present study, the process of oceanic frontal zones could affect atmospheric boundary layer have not diagnosed due to the limited spatial resolution. Long-term high-resolution observation and prescribed coupled model experiments are required to address the detail process of the subarctic oceanic frontal zones influencing the overlying atmospheric boundary layer and the free atmosphere.

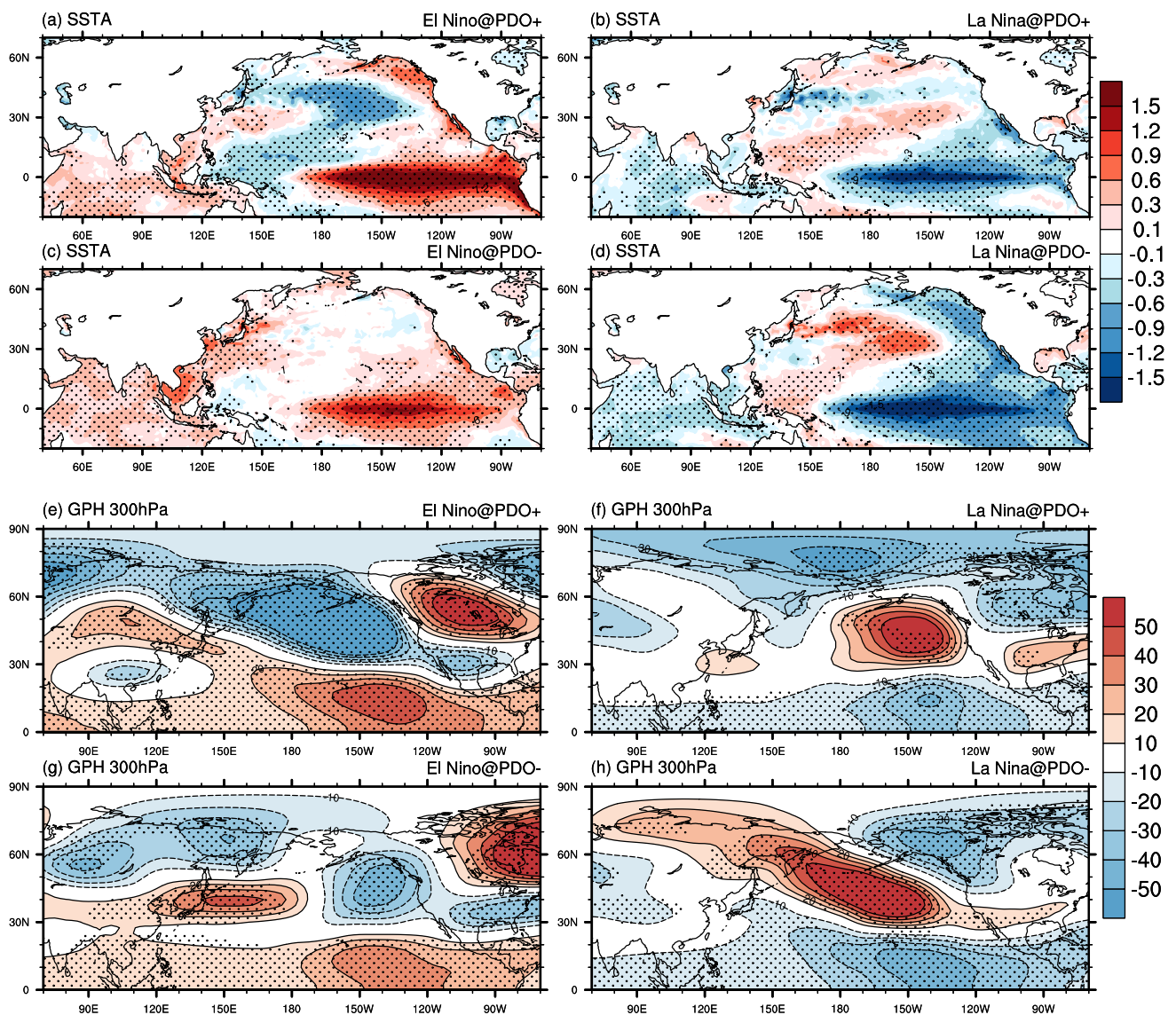


Fig. 14 Composite of SSTA (unit: K) and geopotential height anomalies at 300 hPa (GPH, unit: m) for **a, c, e, f** ENSO warm and **b, d, f, h** cold events in **a, b, e, f** PDO positive and **c, d, g, h** negative phase for

winter of 1950–2010. Stippled areas are statistically significant at the 5% level based on the Student's *t* test

Acknowledgements This work was supported by the National Key Program for Developing Basic Science (Grants 2018YFC1505903, 2016YFA0600303, and 2018YFC1505803) and National Natural Science Foundation of China under Grant No. 41621005, 41505059, 41675064, 41675067, 41875086, and 41330420. The authors are thankful for the support of the Jiangsu Provincial Innovation Center for Climate Change and Fundamental Research Funds for the Central Universities. This work was jointly supported by the Joint Open Project of KLME and CIC-FEMD (Grant KLME201902). The authors would like to thank ECMWF, NOAA, and JISAO for making available the various data used in this study. This work has been benefited from discussions with Prof. William Perrie of BIO. We thank graduate student Shun-Yu Jiang for performing the SSTA simulation. We also thank the reviewers, whose critical comments have led to many improvements in this paper.

Open Access This article is licensed under a Creative Commons Attribution 4.0 International License, which permits use, sharing, adaptation, distribution and reproduction in any medium or format, as long as you give appropriate credit to the original author(s) and the source, provide a link to the Creative Commons licence, and indicate if changes were made. The images or other third party material in this article are included in the article's Creative Commons licence, unless indicated otherwise in a credit line to the material. If material is not included in the article's Creative Commons licence and your intended use is not permitted by statutory regulation or exceeds the permitted use, you will need to obtain permission directly from the copyright holder. To view a copy of this licence, visit <http://creativecommons.org/licenses/by/4.0/>.

References

- Alexander MA, Bladé I, Newman M, Lanzante JR, Lau N-C, Scott JD (2002) The atmospheric bridge: the influence of ENSO teleconnections on air–sea interaction over the global oceans. *J Clim* 15:2205–2231
- Bjerknes J (1969) Atmospheric teleconnections from the equatorial Pacific. *Mon Weather Rev* 97:163–172
- Cai M, Mak M (1990) Symbiotic relation between planetary and synoptic-scale waves. *J Atmos Sci* 47:2953–2968
- Chang EKM, Fu Y (2002) Interdecadal variations in Northern Hemisphere winter storm track intensity. *J Clim* 15:642–658
- Chang EMK, Yau AMW (2016) Northern Hemisphere winter storm track trends since 1959 derived from multiple reanalysis datasets. *Clim Dyn* 47:1435–1454. <https://doi.org/10.1007/s00382-015-2911-8>
- Chang EKM, Lee S, Swanson KL (2002) Storm track dynamics. *J Clim* 15:2163–2183
- Chen W, Yang S, Huang RH (2005) Relationship between stationary planetary wave activity and the East Asian winter monsoon. *Atmos J Geophys Res*. <https://doi.org/10.1029/2004JD005669>
- Chen W, Feng J, Wu RG (2013) Roles of ENSO and PDO in the link of the east asian winter monsoon to the following summer monsoon. *J Clim* 26:622–635
- Chen QY, Hu HB, Ren XJ, Yang X-Q (2019) Numerical simulation of midlatitude upper-level zonal wind response to the change of North Pacific subtropical front strength. *Atmos J Geophys Res*. <https://doi.org/10.1029/2018JD029589>
- Chu CJ, Yang X-Q, Ren XJ, Zhou TJ (2014) Response of Northern Hemisphere storm tracks to Indian-western Pacific Ocean warming in atmospheric general circulation models. *Clim Dyn* 40:1057–1070. <https://doi.org/10.1007/s00382-013-1687-y>
- Chu CJ, Yang X-Q, Sun XG, Yang DJ, Jiang YQ, Feng T, Liang J (2018) Effect of the tropical Pacific and Indian Ocean warming since the late 1970s on wintertime Northern Hemispheric atmospheric circulation and East Asian climate interdecadal changes. *Clim Dyn*. <https://doi.org/10.1007/s00382-017-3790-y>
- Deser C, Wallace JM (1990) Large-scale atmospheric circulation features of warm and cold episodes in the tropical Pacific. *J Clim* 3:1254–1281
- Di Lorenzo E, Liguori G, Schneider N, Furtado JC, Anderson BT, Alexander MA (2015) ENSO and meridional modes: a null hypothesis for Pacific climate variability. *Geophys Res Lett* 42:9440–9448. <https://doi.org/10.1002/2015GL066281>
- Eady ET (1949) Long waves and cyclone waves. *Tellus* 1:33–52
- Fang J, Yang X-Q (2016) Structure and dynamics of decadal anomalies in the wintertime midlatitude North Pacific ocean–atmosphere system. *Clim Dyn* 47:1989–2007. <https://doi.org/10.1007/s00382-015-2946-x>
- Frankignou C, Sennéchal N, Kwon Y-O, Alexander MA (2011) Influence of the meridional shifts of the Kuroshio and the Oyashio Extensions on the atmospheric circulation. *J Clim* 24:762–777
- Gent PR, Danabasoglu G, Donner LJ et al (2011) The community climate system model version 4. *J Clim* 24:4973–4991
- Gershunov A, Barnett TP (1998) Interdecadal modulation of ENSO teleconnections. *Bull Am Meteorol Soc* 79:2715–2725
- Han B, Ren XJ, Yang X-Q (2007) Analysis of the north pacific storm track anomaly and the relationship with zonal wind. *Sci Meteorol Sin* 27(3):237–245
- Hoerling MP, Kumar A, Zhong M (1997) El Niño, La Niña, and the nonlinearity of their teleconnections. *J Clim* 10:1769–1786
- Hoerling MP, Kumar A, Xu T (2001) Robustness of the nonlinear climate response to ENSO's extreme phases. *J Clim* 14:1277–1293
- Horel JD, Wallace JM (1981) Planetary-scale atmospheric phenomena associated with the Southern Oscillation. *Mon Weather Rev* 109:813–829
- Hoskins BJ, Karoly DJ (1981) The steady linear response of a spherical atmosphere to thermal and orographic forcing. *J Atmos Sci* 38:1179–1196
- Hoskins BJ, Valdes PJ (1990) On the existence of storm tracks. *J Atmos Sci* 47:1854–1864
- Hu Z-Z, Huang B (2009) Interferential impact of ENSO and PDO on dry and wet conditions in the US Great Plains. *J Clim* 22:6047–6065
- Jiang SY, Hu HB, Zhang N, Lei LP, Bai HK (2019) Multi-source forcing effects analysis using Liang–Kleeman information flow method and the community atmospheric model (CAM4.0). *Clim Dyn*. <https://doi.org/10.1007/s00382-019-04914-x>
- Koide H, Kodera K (1999) A SVD analysis between the winter NH 500-hPa height and surface temperature fields. *J Meteorol Soc Jpn* 77:47–61
- Kwon Y-O, Alexander MA, Bond NA, Frankignoul C, Nakamura H, Qiu B, Thompson LA (2010) Role of the gulf stream and Kuroshio–Oyashio systems in large-scale atmosphere–ocean interaction: a review. *J Clim* 23:3249–3281
- Lau N-C, Holopainen E (1984) Transient eddy forcing of the time mean flow as identified by geopotential tendencies. *J Atmos Sci* 41:313–328
- Lau N-C, Nath MJ (1991) Variability of the baroclinic and barotropic transient eddy forcing associated with monthly changes in the midlatitude storm tracks. *J Atmos Sci* 48:2589–2613
- Lau N-C, Nath MJ (1994) A modeling study of the relative roles of tropical and extratropical SST anomalies in the variability of the global atmosphere–ocean system. *J Clim* 7:1184–1207
- Lindzen RS, Farrell B (1980) A simple approximate result for the maximum growth rate of baroclinic instability. *J Atmos Sci* 37:1648–1654
- Liu ZY, Alexander M (2007) Atmospheric bridge, oceanic tunnel, and global climatic teleconnections. *Rev Geophys*. <https://doi.org/10.1029/2005RG000172>
- Lorenz DJ, Hartmann DL (2001) Eddy-zonal flow feedback in the Southern Hemisphere winter. *J Atmos Sci* 58:3312–3327
- Lorenz DJ, Hartmann DL (2003) Eddy-zonal flow feedback in the Northern Hemisphere winter. *J Clim* 16:1212–1227
- Mantua NJ, Hare SR, Zhang Y, Wallace JM, Francis RC (1997) A Pacific interdecadal climate oscillation with impacts on salmon production. *Bull Am Meteorol Soc* 78:1069–1079
- McCabe GJ, Palecki MA, Betancourt JL (2004) Pacific and Atlantic Ocean influences on multidecadal drought frequency in the United States. *Proc Natl Acad Sci USA* 101:4136–4141
- Minobe S, Kuwano-Yoshida A, Komori N, Xie S, Small RJ (2008) Influence of the Gulf Stream on the troposphere. *Nature* 452:206–209
- Nakamura H, Kazmin A (2003) Decadal changes in the North Pacific frontal zones as revealed in ship and satellite observations. *J Geophys Res* 108:C33078
- Nakamura H, Nakamura M, Anderson JL (1997a) The role of high- and low-frequency dynamics in blocking formation. *Mon Weather Rev* 125:2074–2093
- Nakamura H, Lin G, Yamagata T (1997b) Decadal climate variability in the North Pacific during the recent decades. *Bull Am Meteorol Soc* 78:2215–2225
- Nakamura H, Sampe T, Tanimoto Y, Shimpo A (2004) Observed associations among storm tracks, jet streams and midlatitude oceanic fronts. In: Wang C, Xie S-P, Carton JA (eds) *Earth's climate: the ocean–atmosphere interaction*, Geophys Monogr Servol 147. AGU, Washington, DC, pp 329–345
- Nakamura H, Sampe T, Goto A, Ohfuchi W, Xie SP (2008) On the importance of midlatitude oceanic frontal zones for the mean state

- and dominant variability in the tropospheric circulation. *Geophys Res Lett* 35:L15709. <https://doi.org/10.1029/2008GL034010>
- Neale RB, Richter JH, Conley AJ et al (2010) Description of the NCAR community atmosphere model (CAM 4.0). Technical Note NCAR/TN-485 + STR
- Newman M et al (2016) The Pacific decadal oscillation, revisited. *J Clim* 29:4399–4427
- Nonaka M, Nakamura H, Tanimoto Y, Kagimoto T, Sasaki H (2006) Decadal variability in the Kuroshio–Oyashio extension simulated in an eddy-resolving OGCM. *J Clim* 19:1970–1989
- Poli P, Hersbach H, Dee DP (2016) ERA-20C: an atmospheric reanalysis of the twentieth century. *J Clim* 29:4083–4097. <https://doi.org/10.1175/JCLI-D-15-0556.1>
- Qiu B, Chen S (2005) Variability of the Kuroshio extension jet, recirculation gyre, and mesoscale eddies on decadal time scales. *J Phys Oceanogr* 35:2090–2103
- Ren XJ, Zhang YC, Xiang Y (2008) Connections between wintertime jet stream variability, oceanic surface heating, and transient eddy activity in the North Pacific. *J Geophys Res* 113:D21119. <https://doi.org/10.1029/2007JD009464>
- Takaya K, Nakamura H (2013) Interannual variability of the East Asian winter monsoon and associated modulations of the planetary waves. *J Clim* 26:9445–9461. <https://doi.org/10.1175/JCLI-D-12-00842.1>
- Trenberth KE, Hurrell JW (1994) Decadal atmosphere–ocean variations in the Pacific. *Clim Dyn* 9:303–319
- Wallace JM, Gutzler DS (1981) Teleconnections in the geopotential height field during the Northern Hemisphere winter. *Mon Weather Rev* 109:784–812
- Wang C (2000) On the atmospheric responses to tropical Pacific heating during the mature phase of El Niño. *J Atmos Sci* 57:3767–3781
- Wang LY, Hu HB, Yang X-Q (2018) The atmospheric responses to the intensity variability of subtropical front in the wintertime North Pacific. *Clim Dyn*. <https://doi.org/10.1007/s00382-018-4468-9>
- Xu HM, Wang LW, He JH (2008) Observed oceanic feedback to the atmosphere over the Kuroshio Extension during spring time and its possible mechanism. *Chin Sci Bull* 53:1905–1912
- Xu HM, Tokinaga H, Xie SP (2010) Atmospheric effects of the Kuroshio large meander during 2004–05. *J Clim* 23:4704–4715
- Xu HM, Xu MM, Xie S-P, Wang Y-Q (2011) Deep atmospheric response to the spring Kuroshio over the East China Sea. *J Clim* 24:4959–4972
- Yao Y, Zhong Z, Yang X-Q (2016) Numerical experiments of the storm track sensitivity to oceanic frontal strength within the Kuroshio/Oyashio extensions. *J Geophys Res Atmos* 121(6):2888–2900
- Zhang LY, Xu HM, Shi N, Deng JC (2017) Responses of the East Asian jet stream to the North Pacific subtropical front in spring. *Adv Atmos Sci* 34:144–156
- Zhu YM, Yang X-Q (2003) Relationships between Pacific Decadal Oscillation (PDO) and climate variabilities in China. *Acta Meteorol Sin* 61:641–654 (in Chinese)

Publisher's Note Springer Nature remains neutral with regard to jurisdictional claims in published maps and institutional affiliations.